ACS SENSORS

pubs.acs.org/acssensors Article

Wearable Cortisol Aptasensor for Simple and Rapid Real-Time Monitoring

Jai Eun An,[‖] Kyung Ho Kim,[‖] Seon Joo Park, Sung Eun Seo, Jinyeong Kim, Siyoung Ha, Joonwon Bae,* and Oh Seok Kwon*

Cite This: *ACS Sens.* 2022, 7, 99−108 Read Online

ACCESS | Metrics & More | Article Recommendations | Supporting Information

ABSTRACT: The necessity of managing stress levels is becoming increasingly apparent as the world suffers from different kinds of stresses including the extent of pandemic, the corona virus disease 2019 (COVID-19). Cortisol, a clinically confirmed stress hormone related to depression and anxiety, affects individuals mentally and physically. However, current cortisol monitoring methods require expert personnel, large and complex machines, and long time for data analysis. Here, we present a flexible and wearable cortisol aptasensor for simple and rapid cortisol real-time monitoring. The sensing channel was produced by electrospinning conducting polyacrylonitrile (PAN) nanofibers (NFs) and subsequent vapor deposition of carboxylated poly(3,4-ethylenedioxythiophene) (PEDOT). The conjugation of the cortisol aptamer on the PEDOT-PAN NFs provided the critical sensing mechanism for the target molecule. The sensing test was performed with a liquid-ion gated field-effect transistor (FET) on a polyester (polyethylene terepthalate). The sensor performance showed a detection limit of 10 pM (<5 s) and high selectivity in the presence of interference materials at 100 times higher concentrations. The practical usage and real-time monitoring of the cortisol aptasensor with a liquid-ion gated FET system was demonstrated by successful transfer to the swab and the skin. In addition, the real-time monitoring of actual sweat by applying the cortisol aptasensor was also successful since the aptasensor was able to detect cortisol approximately 1 nM from actual sweat in a few minutes. This wearable biosensor platform supports the possibility of further application and on-site monitoring for changes of other numerous biomarkers.

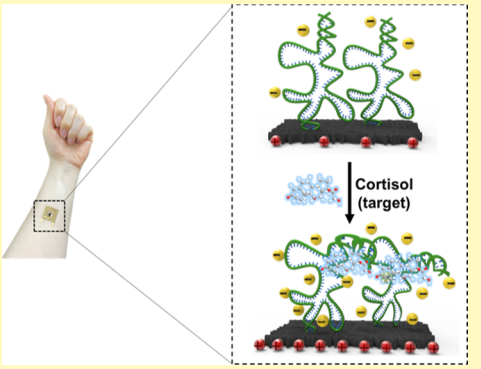

KEYWORDS: *cortisol, aptasensor, flexible, biosensor, wearable, swappable*

People are experiencing different kinds of stresses from the society, personal life, and the extent of COVID-19 pandemic, which continue to deteriorate the psychological health along with the physical health of individuals.[1] Monitoring of stress hormones is important to improve the quality of life; it is particularly essential to monitor cortisol, which plays a core function as a natural alarm system and communicates with brain regions to control the mood and provide motivation. Cortisol is a glucocorticoid steroid hormone derived from cholesterol and is a medically proven stress biomarker that plays significant roles in several psychological functions. Cortisol controls severe and incurable stress responses while maintaining glucose levels, carbohydrate metabolism, and blood pressure. Excess cortisol has a high possibility of causing symptoms such as exhaustion, bone fragility, and obesity, culminating in Cushing's syndrome.[2] On the other hand, insufficient cortisol shows symptoms of weight loss, fatigue, and skin darkening and ultimately Addison's disease.[3] Moreover, the normal range of cortisol varies with time: 136−690 nM in the morning and 55−386 nM in the evening.[4,5] Therefore, monitoring cortisol for one's quality of life is important, especially in this pandemic state. Cortisol is commonly analyzed with electrochemical and enzyme-linked immunosorbent assays (ELISA), gas chromatography−mass spectrometry, radioimmunoassays, surface-enhanced Raman spectroscopy, and ultraviolet spectroscopy.[4,5] Obtaining test results via these methods requires highly trained experts, preparation of large-scale samples, ability to use large and complicated instruments, and extended data analysis time; nevertheless, some of the results obtained by these methods are not reliable.[3,6−9] To overcome the disadvantages of the most commonly used analysis technologies, the development of flexible and wearable electronic devices using wearable materials has recently become attractive due to their unique characteristics, such as high flexibility, excellent mechanical properties, and elasticity, and their wide applications in the fields of human health and emotion monitoring.[10−17] With

Received: August 15, 2021
Accepted: December 28, 2021
Published: January 7, 2022

https://doi.org/10.1021/acssensors.1c01734
ACS Sens. 2022, 7, 99−108

these extraordinary properties, the silk substrate is proven to play a critical role as an efficient medium for transferring materials such as metallic electrodes onto tissues by dissolution.[18] However, the development of sensors possessing high flexibility, sensitivity, and stability toward specific biomarkers is still a challenging task since there is little research on the direct monitoring of biological systems. Furthermore, there is a great demand for flexible and wearable sensors that can be integrated into clothing or mounted on the skin for various purposes, such as diagnosis, therapy, and remote control, which shows the need for simple, accurate, and rapid detection.[19−22]

With cortisol detection being studied extensively, a new and novel wearable biosensor platform to detect cortisol was designed in this study.[23−29] We demonstrated a wearable and even swappable cortisol aptasensor. The silk substrate has characteristics such as high flexibility, easy disposal, and an amorphous nature, enabling transfer to other substrates.[30−32] In addition, the aptasensor showed great flexibility as there was no loosening or cutting of the metallic pattern when it was bent. The excellent function of the cortisol aptasensor was characterized after transfer to polyethylene terephthalate (PET). The cortisol aptasensor consisted of aptamer-conjugated poly(3,4-ethylenedioxythiophene) (PEDOT)-polyacrylonitrile (PAN) nanofibers (NFs), which were used as a channel as they were proven for cortisol detection in previous studies and showed high performance with a detection limit of 10 pM and high selectivity in the presence of several interfering materials at concentrations 100 times higher than that of cortisol.[33−37] This extends the high potential utility of swappable and wearable cortisol aptasensors. These results introduce the possibility of a portable and on-site monitoring system by being successfully applied on various substrates.

MATERIALS AND METHODS

Materials. Chemicals for nanofiber preparation, such as lithium bromide (LiBr), sodium carbonate (Na_2CO_3), iron(III)chloride ($FeCl_3$), PAN (average MW = 150,000 kg/mol), 3,4-ethylenedioxythiophene (EDOT), carboxylated 3,4-ethylenedioxythiophene (EDOT-COOH), dimethylformamide (DMF) as a solvent, 4-(4,6-dimethoxy-1,3,5-triazin-2-yl)-4-methylmorpholinium chloride (DMT-MM) as a condensing agent, cysteine, cortisol, corticosterone, prednisolone, and cortisone, were purchased from Aldrich (Milwaukee, WI, USA) and used without further purification. A cortisol aptamer with the sequence 5′-ATG GGC AAT GCG GGG TGG AGA ATG GTT GCC GCA CTT CGG C/3AmMO/-3′ was synthesized by IDT (Coralville, IA, U.S.). Artificial saliva (1700−0303) and artificial sweat (1700−0506) were purchased from Insung Chromatech (South Korea).

Preparation of PAN NFs by Electrospinning. PAN was dissolved in DMF to obtain a precursor solution (10 wt %) and stirred gently at approximately 75 °C to promote dissolution. Subsequently, the homogeneous precursor solution was injected by a disposable syringe connected to an electrospinning machine (ESR 200R; NanoNC, Seoul, Korea). An electric field of 15−20 kV was applied between the needle gap and a flat collector covered with an aluminum foil. The distance between the syringe tip and the grounded flat collector was 20 cm, and the flow rate was adjusted to 1.0 mL/h. All electrospinning was conducted within a chamber, and the product was collected for 4 h.[33]

Vapor Deposition Polymerization of EDOT/EDOT-COOH on PAN NFs. PAN NFs were soaked in aqueous initiator solution ($FeCl_3$, 10 wt %) for wetting and then dried completely. Next, the NFs were moved to a flask-type reactor with a sealing apparatus designed for vapor deposition polymerization (VDP). The reactor containing the monomer mixture [EDOT (90 wt %)/EDOT-COOH (10 wt %)] was evacuated at room temperature, and a vacuum was applied inside the reactor. Subsequently, the monomer mixture was vaporized by heating the reactor at 70 °C. VDP proceeded for 24 h at this temperature in the atmosphere of the vaporized monomer. After polymerization, the residual monomer was removed from the reactor by venting.

Fabrication of Silk Film. *Bombyx mori* cocoons were boiled in aqueous Na_2CO_3 solution (0.02 M) for 30 min to remove the rubbery constituents. The solid residue was washed in distilled water (DW) and dried at room temperature for 12 h. The obtained cocoon skein (1 g) was dissolved in aqueous LiBr solution (9.3 M, 4 mL), and the prepared solution was dialyzed in DW for 2 days to remove excessive salt. The solution was ultracentrifuged at 10,000 rpm, and the final obtained fibroin solution was stored at 4 °C. Finally, a transparent silk film with a thickness of approximately 40 μm was produced by casting the fibroin solution on a substrate (Figure S1).[38]

Fabrication of PEDOT-PAN NF Cortisol Aptasensor. The electrodes of a source/drain line of 100 μm width, 40 μm gap, and Au with a thickness of 150 nm on the thin silk film were patterned by an electron beam (E-Beam, ZZZ550-2, Maestech) evaporator through a patterned shadow mask. To immobilize PEDOT-PAN NFs on the electrodes, cysteine was coated on the electrodes using SH-Au binding, and the carboxyl group of PEDOT-PAN NFs reacted with 1 wt % DMT-MM to bond the NFs with the cysteine.[39] The obtained electrodes were dispersed using DW. The NFs conjugated with the coupling agent (DMT-MM) and 10 μM cortisol aptamer were attached at the center of the electrodes. The coupling reaction to attach the aptamers to the NFs proceeded for 1 h. To transfer the silk substrate-based electrodes onto the applicable substrate, the silk film was loaded on the substrate and then dissolved using DW for approximately 3 min.

Characterization. The cortisol aptamer was labeled with fluorescein-5-isothiocyanate (FITC) at the 5′ or 3′. FITC-labeled and nonlabeled aptamers were immobilized on PEDOT-PAN NFs, and fluorescence images of the aptamer-functionalized PEDOT-PAN NFs were obtained by an Evos FL instrument (Thermo Fisher Scientific Corporation). Fourier transform infrared spectroscopy (FT-IR) and Raman spectra were recorded on FT-IR (Alpha-P) and Raman (BX41RF-LED Olympus, 633 nm laser) spectrometers, respectively. Scanning electron microscopy (SEM) micrographs were obtained with an MSE20 scanning electron microscope at an accelerating voltage of 10 kV. The microstructure of the silk film was analyzed using X-ray diffraction (XRD) (SmartLab, Rigaku Co.), and the thermal stability of the silk film was measured by thermal gravimetric analysis (TGA) (TGA 93-18, Setaram, France).

Sensing Tests. To determine the sensor performance, the cortisol aptasensor was transferred on a PET film, swab, and skin using DW, and then 4 μL of 10 μM cortisol aptamer conjugated with PEDOT-PAN NFs.[40] Next, a chamber was attached to the aptamer-conjugated PEDOT-PAN NFs, and the chamber was filled up using 10 μL of phosphate-buffered saline (PBS) solution.[33,35] Subsequently, cortisol diluted in PBS solution was dropped to the aptamer-conjugated NFs to observe the electrical characteristics. For further application using the swab and the skin using a liquid-ion gated system, cortisol was diluted with artificial saliva and artificial sweat by concentration.

Actual sweat-sensing test was performed through a side-gated system which is an advanced setup system since this system is used for monitoring cortisol from a moving person.

A Keithley 2612A SourceMeter was used to obtain the real-time response. The current change was normalized according to the equation $\Delta I/I_0 = (I - I_0)/I_0$, where I_0 is the initial real-time current and I is the measured real-time current.

ELISA Test. To verify the cortisol concentration in the actual sweat sample, the ELISA test (KA1885, Abnova, Taiwan) was performed. 50−100 μL of actual sweat was collected using obstructed one-to-three layers of bandage, and 50 μL of each sample was used for ELISA kit based on the competitive binding principle.[41−43] Each sample was dispensed in the polyclonal rabbit antibody coated well and incubated with the enzyme conjugate (cortisol conjugated to horseradish peroxidase). Endogenous cortisol of each sample competes with the

https://doi.org/10.1021/acssensors.1c01734
ACS Sens. 2022, 7, 99−108

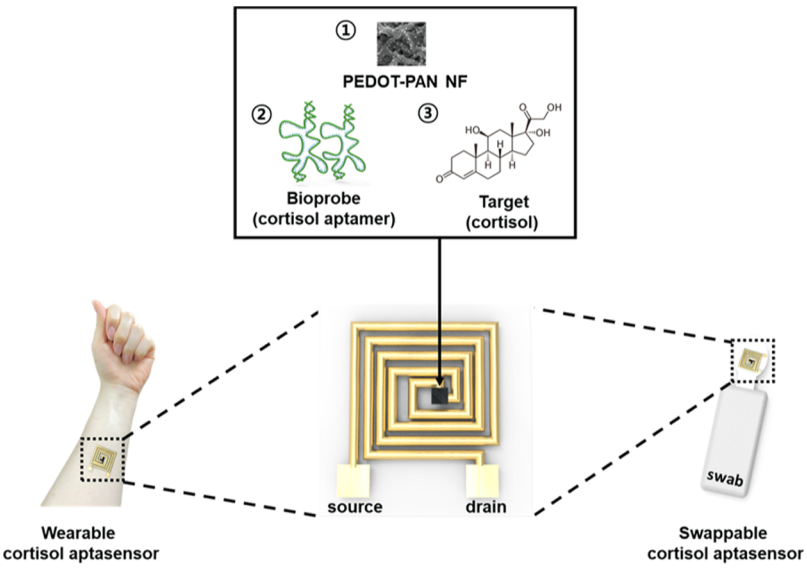

Figure 1. Schematic illustrations of the overall schematic illustration of the cortisol aptasensor.

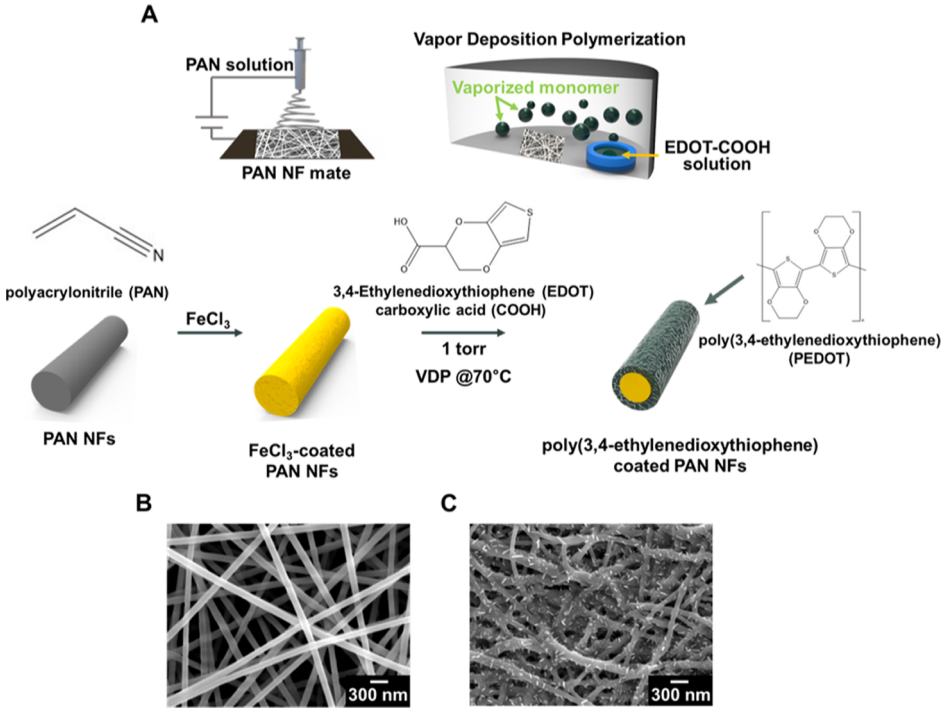

Figure 2. Fabrication of PAN NFs. (A) Schematic illustration of PAN NF VDP fabrication by electrospinning. Field emission SEM images of the (B) pristine PAN template and (C) polymerized PEDOT coated on the PAN NF surface.

enzyme conjugate for antibody binding during the incubation. Subsequently, the substrate solution was added, and the color development and absorbance were measured at 450 nm with a microtiter plate reader.

RESULTS AND DISCUSSION

Overall Concept of the Cortisol Aptasensor. Figure 1 shows the concept of the silk substrate-based cortisol aptasensor. The cortisol aptasensor is composed of a patterned Au electrode with a source and drain, and PEDOT-PAN NFs are shown at the center. The PEDOT-PAN NFs acted as the sensor channel after it conjugated with a specific bioprobe (cortisol aptasensor) to detect the target (cortisol). The illustrations on the left and right show the cortisol aptasensor for wearable (left) and swappable (right) applications.

Fabrication of PEDOT-PAN NFs. Figure 2A shows a schematic diagram representing sequential electrospinning and VDP processes for the preparation of conducting PEDOT-PAN NFs, which play a critical role as channels in the cortisol aptasensor. First, PAN NFs were produced by a conventional electrospinning process, which acted as a backbone for the preparation of the sensing medium. Although diverse polymers could be used for this purpose, PAN was selected because it is suitable for electrospinning and has several advantages, such as chemical inertness, thermal stability, and mechanical durability. In addition, PAN is stable under acidic/basic conditions and

https://doi.org/10.1021/acssensors.1c01734
ACS Sens. 2022, 7, 99−108

insoluble in most common solvents. Moreover, the presence of rigid semicrystalline domains renders mechanical robustness. Figure 2B shows the SEM image of pristine PAN NFs with a sufficiently large aspect ratio produced by the electrospinning apparatus. It is remarkable that the beads are apparently absent in the PAN NFs. This aspect is desirable for the construction of a sensor because the irregular formation of beads might be a physical hindrance to signal transduction during sensor measurement.

Subsequently, a PEDOT layer was incorporated on the surface of the PAN NFs by a simple VDP process. As the feasibility of the VDP process was demonstrated previously, it was expected that a uniform PEDOT layer would be generated spontaneously.[33] Figure 2C shows the SEM image of the PEDOT-PAN NFs obtained through the sequential procedure. The structural features of the PAN NFs were almost completely retained after the VDP process. However, the surface appearance of the PEDOT-PAN NFs was different from that of the PAN NFs. First, the surface roughness increased due to variation in the PEDOT layer thickness. Even if the reactivity of the EDOT-COOH monomer undergoing electrochemical polymerization was lower than that of EDOT, the overall reaction for the formation of PEDOT was spontaneous and relatively fast due to the high reduction potential of $FeCl_3$, which increased the surface area. The formation of needle-type residues was attributed to the presence of initiator ($FeCl_3$) crystallites. The polymerization could be accelerated locally at sites where the initiator concentration was relatively high.

Characterization of the Cortisol Aptasensor. Figure 3A presents an image of the cross-sectional SEM image of the obtained silk film showing the internal morphology along with the optical image showing the ultralight weight of the silk film. The image clearly shows the polymeric domains and free voids; however, it is difficult to understand the microstructure. Therefore, it was necessary to further analyze the microstructure of the silk film using XRD, as shown in Figure 3B. The silk film showed a broad peak from 12.0° showing an amorphous structure.[44] This feature might contribute to the flexibility and optical transparency. In Figure 3C, the thermal stability of the obtained silk film was examined with the TGA equipment. A typical profile of polymeric materials was obtained, showing a slow and gradual removal of residues and volatile components below 100 °C. Sudden degradation occurred above 250 °C, indicating that the film possessed sufficient thermal stability as a sensor substrate.[45] Remarkably, the residual mass fraction was relatively high. This might be associated with the microstructure stability due to prevalent specific interactions, such as hydrogen bonding.

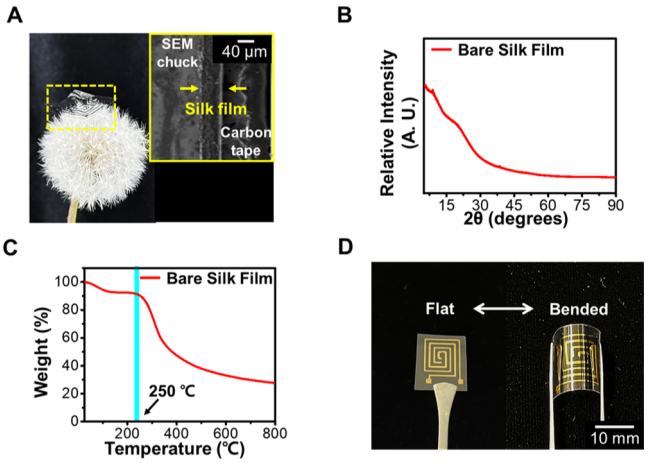

Figure 3. Characterization of the cortisol aptasensor. (A) Optical image of the ultralight-weight electrode with field emission SEM images of the silk film thickness. (B) XRD of the unmodified silk film. (C) Thermal analysis of the unmodified silk film using TGA. (D) Optical image showing the flexibility of the silk substrate-based electrode transferred onto the PET film before the application of PEDOT-PAN NFs and real-time monitoring using a liquid-ion gated system.

An Au electrode patterned by deposition on a silk substrate was used as the base of the cortisol aptasensor. It was transferred to the PET film, and the silk was dissolved, leaving only the Au pattern. Then, cortisol aptamer-conjugated PEDOT-PAN NFs were attached. The optical image in Figure 3D clearly shows the flexibility and water-solubility characteristics after transfer to the PET film, where no breakage or loss of the Au pattern was shown.

Characterization of Immobilized Bioprobes. The next step to obtain the sensor system was conjugating the cortisol aptamer to the surface of the PEDOT-PAN NFs, which was an important prerequisite for subsequent experiments. The aptamer molecules were conjugated to the PEDOT-PAN NFs using a condensing agent, leading to the formation of amide bonds between carboxylic acid and amine groups. Successful incorporation of the aptamers was confirmed with the fluorescence microscope images of pristine and FITC-labeled aptamer-conjugated NFs (Figure 4A). No significant fluorescent image was observed for the pristine NFs (left), while the FITC-labeled aptamer-conjugated NFs showed clear fluorescent emission (right).

Further spectroscopic analysis was conducted to confirm the effective introduction of the aptamers as presented in Figure 4B. To confirm the formation of covalent bonds between COOH in NFs and NH in aptamers, FT-IR spectra were

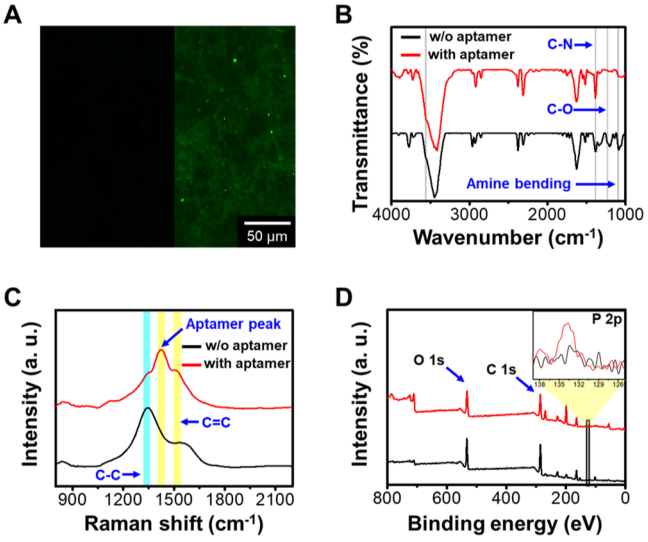

Figure 4. Characteristic of aptamer immobilization. (A) Fluorescent images of pristine NFs (left) and NFs with FITC labeled on the aptamer (right). (B) FT-IR spectroscopy of pristine NFs (black) and aptamer-conjugated NFs (red). (C) Raman spectra of pristine NFs (black) and aptamer-conjugated NFs (red). (D) XPS spectra before (black) and after (red) aptamer conjugation on NFs.

https://doi.org/10.1021/acssensors.1c01734
ACS Sens. 2022, 7, 99−108

obtained before and after aptamer functionalization. Major changes were observed at the peaks associated with the occurrence of amide groups. The peak at 3500 cm^{-1} due to N−H became stronger after the attachment of aptamers. The peak intensity at 1400 cm^{-1} originating from C−N stretching also increased; in contrast, the peak at 1350 cm^{-1} associated with C−O stretching became weak. The amine bending peak at 1200 cm^{-1} decreased significantly after aptamer introduction. These characteristics supported the formation of amide groups. The other common peaks remained nearly unchanged before and after aptamer attachment.[46]

Complementary Raman spectra are presented in Figure 4C to further support the successful formation of aptamer-conjugated NFs. It is obvious that the peak intensity at 1350 cm^{-1} decreased, while the intensity at 1400 cm^{-1} increased. These changes in characteristic peaks indicated that amide formation by aptamer attachment was effective.[47,48] This trend was also consistent with the findings from the FT-IR spectra.

Additional convincing evidence was provided by the X-ray photoelectron spectroscopy (XPS) analysis. As the aptamer is composed of a series of amino acids and some of the constituent amino acids contain the element phosphorus (P), XPS analysis was conducted focusing on the electrons in the 2p orbital of phosphorus. The spectrum in Figure 4D shows that the peak intensity at approximately 134 eV increased noticeably after aptamer addition, while there was no significant P 2p peak in the spectrum of the pristine NFs.[49] This result indicates that the phosphorus content increased, supporting the attachment of a substantial amount of the aptamer.

Electrical Property Characterization of Cortisol Aptasensor. The first step in studying the sensor performance by electrical measurement is examining the electrical contact between bioprobes with (red) and without (black) aptamer conjugation on PEDOT-PAN NFs based on the ohmic relation. Figure 5A displays the $I-V$ values before and after aptamer conjugation. Here, the $I-V$ curve for the flexible surface NF aptasensor was observed to be linear over a voltage range of −1.0 to +1.0 V showing excellent ohmic behavior. With the increase in resistance caused by aptamer binding, the conductivity of the unmodified NFs was higher than that of the aptamer-conjugated PEDOT-PAN NFs. The ohmic contact was still present after the attaching and washing steps during the surface functionalization procedures. This indicates that the covalent immobilization of the PEDOT-PAN NFs and the cortisol aptasensor on the Au electrode produced a dependable electrical connection.

A schematic illustration of the liquid-ion gated field-effect transistor (FET) system to characterize the cortisol aptasensor is shown in Figure 5B. PEDOT-PAN NFs, coated with cysteine for SH-Au binding, conjugated with the cortisol aptamer were attached to the cortisol aptasensor after successful transfer of the silk substrate-based cortisol aptasensor onto the PET film for the sensing test. The cortisol aptasensor is composed of a source, drain, and gate electrode for electrical measurement to be used in the FET system. The scheme indicates that the sensing medium was surrounded with a liquid such as PBS (pH 7.4) as an electrolyte to support the formation of a field affected by the supplied gate voltage as a dielectric.

The sensing mechanism of the cortisol aptasensor is shown in Figure 5C. When cortisol, the target material, binds with the aptamer, it is known to have structural reorientation by moving

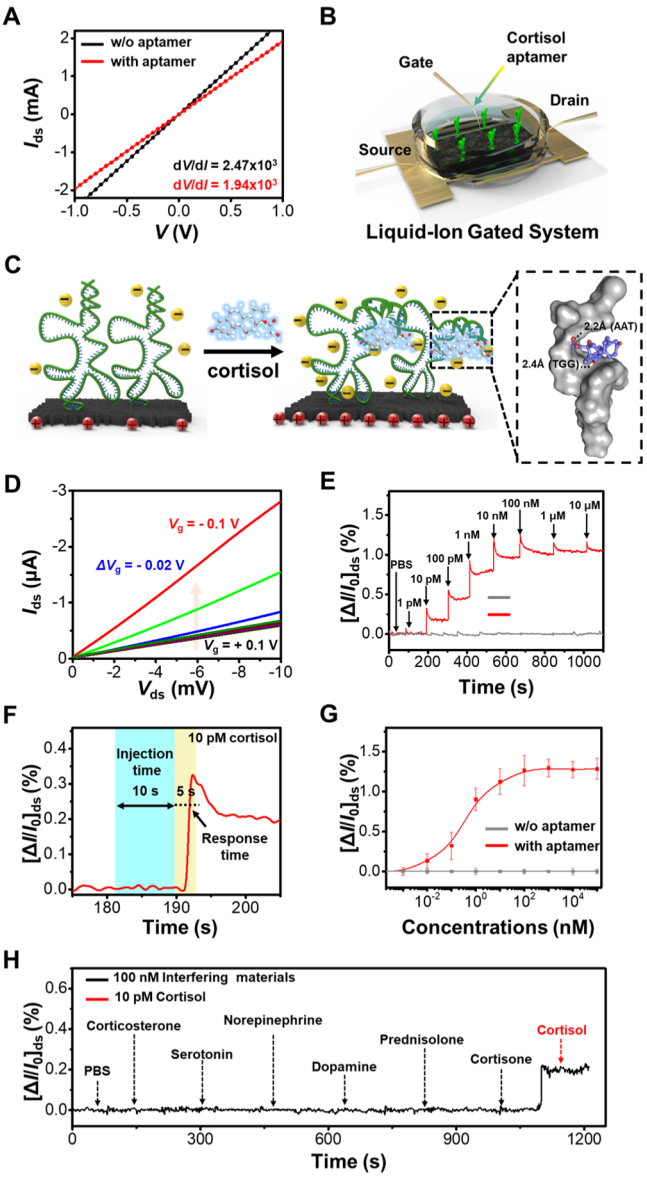

Figure 5. Electrical properties of the cortisol aptasensor. (A) $I-V$ curves of NFs with and without the aptamer. (B) Schematic illustration of the liquid-ion gated cortisol aptasensor consisting of source/drain and gate electrode with the reaction chamber after transfer of the cortisol aptasensor onto the PET film. (C) Binding mechanism between cortisol and the aptamer with 3D structure pose obtained from simulation. (D) $I_{ds}-V_{ds}$ output characteristics of the cortisol aptasensor ranging from −0.1 to 0.1 V in a step 0.02 V of gate voltage (V_{ds} = 0 to −10 mV). (E) Real-time responses using different concentrations of the cortisol aptasensor (1 pM to 10 μM). (F) Real-time response to 10 pM cortisol: injection time (10 s), response time (5 s). (G) Concentration curve of the cortisol aptasensor. (H) Discrimination of cortisol (10 pM) from 100 nM interfering materials.

closer to the p-type channel.[48] To further prove the mechanism, the biosimulation system was performed. The structure presented at the right side of Figure 5C is a pose obtained through a docking program (AutoDock1.5.6). This pose is shown to have two binding sites with the lengths of 2.2 Å-ATT and 2.4 Å-TGG that performed hydrogen bonding. The binding sites showed a high affinity of −6.0 kcal/mol which made the aptamer reoriented toward the structure when the target moved closer to the channel.

https://doi.org/10.1021/acssensors.1c01734
ACS Sens. 2022, 7, 99−108

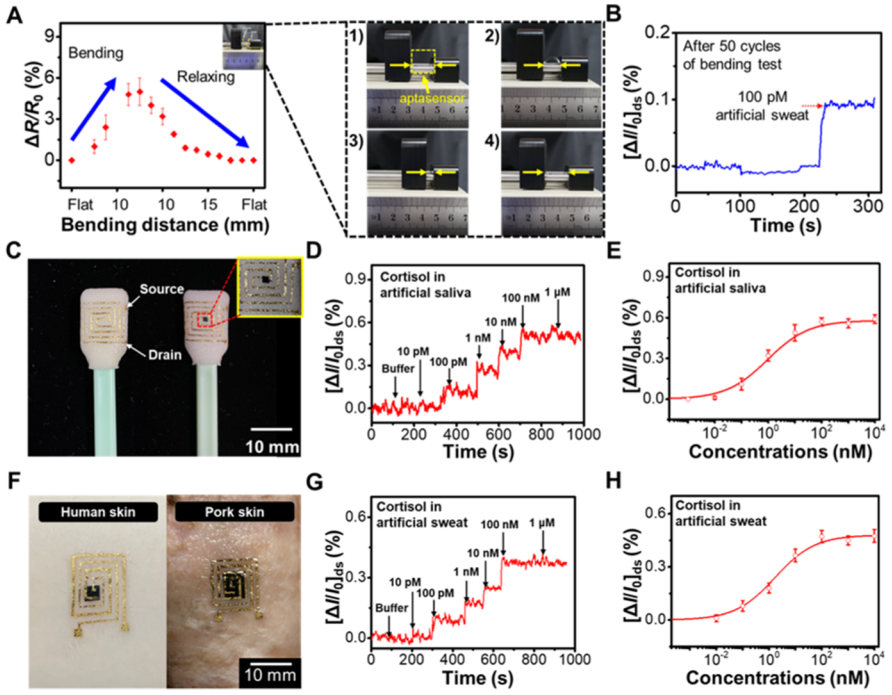

Figure 6. Wearable cortisol aptasensor. (A) Resistance variation of the wearable cortisol aptasensor by changing the bending distance. (B) Real-time monitoring of the cortisol aptasensor after 50 cycles of changing the bending distance. (C) Optical image of the swappable cortisol aptasensor. (D) Real-time response monitored using a liquid-ion gated FET system with artificial saliva on swabs. (E) Calibration curve of the cortisol aptasensor using cortisol in artificial saliva. (F) Optical image of the wearable cortisol aptasensor on the human and pig skin. (G) Real-time response monitored using a liquid-ion gated FET system with artificial sweat on the skin. (H) Calibration curve of the cortisol aptasensor using cortisol in artificial sweat.

To establish the range of p-type operation of the PEDOT-PAN NF cortisol aptasensor, Figure 5D shows the output curve of the liquid gated aptasensor operated with various gate voltages. The drain-to-source current (I_{ds}) negatively increased with negatively increasing gate V_g (in the range of V_{ds} = 0 to −10 mV). In addition, the transfer curve was monitored with −100 mV (red) and −300 mV (blue) of V_{ds} to illustrate the transfer characteristics (I_{ds}−V_g) of the cortisol aptasensor indicating a p-type characteristic since it showed hole-transporting behavior (Figure S2). This phenomenon was critical to prove that the real-time sensing experiment was performed in the p-type region.[26,50−52]

Conformational change happens when the aptamer binds to cortisol, the target material. Reconstruction of the aptamer starts to be reformed nearer to the surface of the NFs, which work as the channel.[53] As the overall feasibility of the aptasensor system was confirmed by the previous results, the major sensor performance, such as sensitivity, linear range, detection limit, and selectivity, was subsequently investigated. Figure 5E shows the real-time response of the PEDOT-PAN NF cortisol aptasensor before (gray) and after (red) aptamer conjugation toward various cortisol concentrations. First, PEDOT-PAN NFs without aptamer conjugation were introduced for control experiments and showed no substantial responses. On the other hand, the response of the aptamer-conjugated PEDOT-PAN NFs showed an intensity surge from 10 pM. Analogous surge patterns were observed consistently above this concentration. Therefore, it was inferred that the detection limit was 10 pM. The obtained limit of detection of the presented aptasensor is approximately 3 times lower compared with other biosensors reported in previous studies with cyclic voltammetry, lateral flow assay, ELISA, and FET (Table S1).

Figure 5F shows the injection and response time of 10 pM cortisol, which showed remarkable peak in real-time monitoring. Injection time is from the moment when the target was dropped to the aptasensor until the current change followed by the response time. Here, the response time was defined from the current change moment up to its 80% of change before saturation.[54] When 10 pM cortisol was injected to the cortisol aptasensor, it responded within 5 s. The rapid response time happened since 10 pM cortisol diffused fast. The rapid response could be explained in terms of sensor formation and specific interaction between the aptamer and the target since PBS solution existed in a chamber, and cortisol was introduced as a form of PBS solution. Therefore, the potential hindrance to interfere with target diffusion to the cortisol aptamer-conjugated aptasensor must be absent. Furthermore, migration of the added cortisol molecules with electron-rich moiety to the NF surface was favorable due to electrostatic interaction. When the target molecule reached the aptasensor, two major phenomena could happen. First is the direct deposition of the target on to the PEDOT-PAN NFs. For this case, it was difficult to observe charge transport phenomenon due to the absence of a specific interaction. On the other hand, specific interactions between the aptamer-conjugated PEDOT-PAN NFs and the target could be promoted and become prevalent. Once the target reached the aptamers, specific interactions occurred spontaneously and charge transport was induced. Consequently, a sharp peak appeared after a relatively short response time (5 s).[55,56]

To quantize the intensity increases as a function of concentration and determine the detection limit quantitatively,

https://doi.org/10.1021/acssensors.1c01734
ACS Sens. 2022, 7, 99−108

the normalized sensitivity to various cortisol concentrations was evaluated and is shown in Figure 5G. The profile for the PEDOT-PAN NFs without aptamer conjugation (gray) showed no significant reaction to various concentrations of cortisol (1 pM to 10 μM).[57,58] In contrast, the profile for the aptasensor showed a substantial value at 10 pM and increased abruptly to 100 nM. Then, the increase terminated above 100 nM; consequently, the linear response range was approximately determined to be 1 pM to 10 μM.

It was also found that the aptasensor boasted excellent selectivity in the presence of similar interfering materials. The selectivity of the aptasensor toward cortisol was demonstrated using the abovementioned compounds. Figure 5H shows that there was a discernible response only after the introduction of cortisol, which enabled the discrimination of cortisol from interfering materials such as steroid hormones (corticosterone, cortisone, and prednisolone) and other neurotransmitters implicated in depression (serotonin, norepinephrine, and dopamine).[45,59]

Applications of the Cortisol Aptasensor. To determine that the electrical characteristic does not change even when the cortisol aptasensor is being bent, bending test was conducted as shown in Figure 6A with enlarged actual image of the bending test in Figure S3. The resistance slightly increased to a bending distance (Δlength/length$_0$) of 5 mm. However, the resistance was completely recovered to the original level after relaxing up to 15 mm.[35,60,61] The real-time monitoring was demonstrated after running 50 cycles of the bending test as shown in Figure 6B. In this figure, a little resistance occurred, yet the *s* is 1/10 compared to the signal after the target was introduced.

The potential application of the cortisol aptasensor as a flexible and wearable device was demonstrated by the introduction of the sensor onto swabs (cotton) and skin. Figure 6C shows the sensor system with a patterned electrode of the cortisol aptasensor applied on a swab. The compatibility between swabs composed of cotton and silk substrate was required to be favorable because detachment of the silk substrate was macroscopically absent. In addition, dewetting of the Au electrode was nonsignificant, leading to stable sensor performance. The sensitivity test of the sensor on a swab was conducted using a liquid-ion gated FET system, which is the same method used in previous sections. Figure 6D shows that the sensor signal was less conspicuous because of the surface roughness; consequently, the sensitivity decreased slightly as remarkable peaks were observed above 100 pM. In addition, the sharpness of the primary peaks decreased. The calibration curve of cortisol in artificial saliva is shown in Figure 6E to assess the intensity change to verify the detection limit and to verify the function of the cortisol aptasensor transferred to a swab.

The cortisol aptasensor was also introduced onto the human skin, and an analogous sensitivity test was performed (Figure 6F). The detection limit was similar to the value obtained in Figure 5B. While the surface of a swab is parabolic and symmetric, the human skin is asymmetric. Therefore, the obtained sensor signal was relatively unstable, and the fluctuation became stronger (Figure 6G). In Figure 6H, the calibration curve of cortisol in artificial sweat is presented, and this determines the function of the cortisol aptasensor toward the sweat sample with normalized sensitivity to various cortisol concentrations in artificial sweat.

Figure 7A shows the illustration of the side-gated system used to monitor cortisol from the actual sample (left), and the

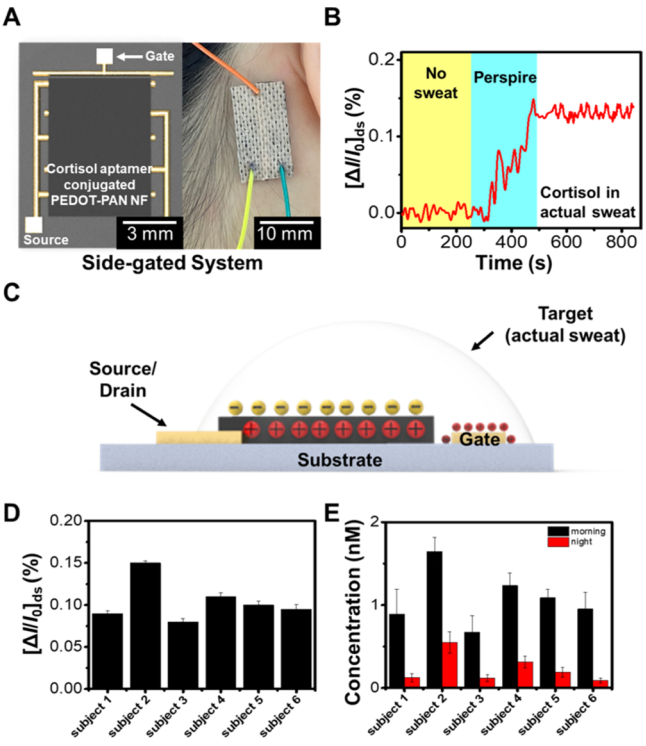

Figure 7. Application of the wearable cortisol aptasensor for detection of cortisol in actual sweat. (A) Illustration of the side-gated system cortisol aptasensor and the optical image of the side-gated system cortisol aptasensor to detect cortisol in actual sweat. (B) Real-time monitoring using an actual sweat sample of subject 2. (C) Schematic illustration of the side-gated system mechanism. (D) Bar graph comparing the intensity change of the subjects' actual sweat sample. (E) ELISA results of the subject in morning (black) and night (red) after cycling.

optical image shows the patched aptasensor at the back of one's ear (right) to be attached near the hair since hair cortisol is known to be a sufficient maneuver of stress.[62−64] Side-gated system was applied to detect cortisol from the actual sample since it is not possible to place the probe tip using the liquid-ion gated system in the covered system.[65−67] The cortisol measurement of the actual sweat was performed after vigorous exercise (cycling) early in the morning, when the cortisol level is the highest in a day, and at night when the cortisol level is the lowest in a day.[12,68−70] The real-time monitoring presented in Figure 7B was performed while subject 2 was cycling vigorously to get extra stress. The no sweat part in the real-time response is when stress was given but not detected through the aptasensor since there was no cortisol given to the aptasensor, while the perspiration part is when the aptasensor started to detect cortisol. Figure 7C presents the mechanism of the side-gated system. This shows that the sweat functions as an electrolyte and covered both the channel and the gate which made it possible to control on the same surface. Moreover, Kapton tape was used to work as an insulator to not disturb the sensing signal.

In Figure 7D, the intensity comparison between the subjects shows that this cortisol aptasensor can demonstrate the difference in cortisol levels from different individuals. ELISA was performed using the collected actual sweat samples to

https://doi.org/10.1021/acssensors.1c01734
ACS Sens. 2022, 7, 99−108

analyze the concentration used in real-time monitoring (Figure 7E). The absorbance showed that the actual sample was approximately 1 nM. Considering these observations, the cortisol aptasensor can be used as a flexible and wearable device.

CONCLUSIONS

In this study, a flexible and wearable aptasensor composed of a PEDOT-PAN NF layer was successfully produced on a silk substrate to detect a typical stress hormone, cortisol. Electrical measurements showed that the sensor exhibited stable and reliable electrical characteristics such as ohmic behavior, a transition curve, and a signal intensity proportional to the concentration. The electrode-type sensor showed superior performances, such as sensitivity (10 pM) and selectivity. Remarkably, the performances were retained substantially when the sensor was transplanted on the swab and the human skin and even to a perspiring moving person. This study will provide important information for future relevant research activities regarding ultralight wearable and disposable devices with a negligible environmental burden. A more extensive study is required to further support the possibility of producing ultralight wearable sensors on silk substrates. By careful interpretation and use of the obtained results, it will be possible to produce more sophisticated biosensors detecting a critical biomarker, cortisol. Moreover, this study can provide a good and substantial idea to develop an effective strategy for the diagnosis of diseases related to cortisol concentration fluctuation.

ASSOCIATED CONTENT

Supporting Information

The Supporting Information is available free of charge at https://pubs.acs.org/doi/10.1021/acssensors.1c01734.

Performance comparison data of various biosensors for cortisol detection, schematic diagram of the silk film fabrication procedure, transfer curve of the PEDOT-PAN NF cortisol aptasensor, and enlarged actual photograph of the wearable cortisol bending test (PDF)

AUTHOR INFORMATION

Corresponding Authors

Joonwon Bae − *Department of Applied Chemistry, Dongduk Women's University, Seoul 02748, Republic of Korea*; Email: joonwonbae@gmail.com, redsox7@dongduk.ac.kr

Oh Seok Kwon − *Infectious Disease Research Center, Korea Research Institute of Bioscience and Biotechnology (KRIBB), Daejeon 34141, Republic of Korea; Nanobiotechnology and Bioinformatics (Major), University of Science & Technology (UST), Daejeon 34141, Republic of Korea;* orcid.org/0000-0002-5936-244X; Email: oskwon79@kribb.re.kr

Authors

Jai Eun An − *Infectious Disease Research Center, Korea Research Institute of Bioscience and Biotechnology (KRIBB), Daejeon 34141, Republic of Korea*

Kyung Ho Kim − *Infectious Disease Research Center, Korea Research Institute of Bioscience and Biotechnology (KRIBB), Daejeon 34141, Republic of Korea;* orcid.org/0000-0003-3587-0877

Seon Joo Park − *Infectious Disease Research Center, Korea Research Institute of Bioscience and Biotechnology (KRIBB), Daejeon 34141, Republic of Korea*

Sung Eun Seo − *Infectious Disease Research Center, Korea Research Institute of Bioscience and Biotechnology (KRIBB), Daejeon 34141, Republic of Korea*

Jinyeong Kim − *Infectious Disease Research Center, Korea Research Institute of Bioscience and Biotechnology (KRIBB), Daejeon 34141, Republic of Korea*

Siyoung Ha − *Infectious Disease Research Center, Korea Research Institute of Bioscience and Biotechnology (KRIBB), Daejeon 34141, Republic of Korea*

Complete contact information is available at: https://pubs.acs.org/10.1021/acssensors.1c01734

Author Contributions

‖J.E.A. and K.H.K. contributed equally.

Author Contributions

O.S.K. and J.B. initiated the study. J.E.A. and K.H.K. performed the fabrication of sensing platforms, measured the real-time responses, characterized the sensing electronics, demonstrated the sensing mechanism, and wrote the manuscript. S.J.P. advised MEMS process to design the electronics. J.K. and S.E.S. prepared the experimental materials and analyzed the experiments. S.H. performed biosimulation and analysis. J.B. provided manuscript feedback and edited the manuscript. O.S.K. conceived and supervised the project

Notes

The authors declare no competing financial interest.

ACKNOWLEDGMENTS

This research was supported by the Defense Acquisition Program Administration (ADD-911255201).

REFERENCES

(1) Ustun, G. Determining Depression and Related Factors in a Society Affected by COVID-19 Pandemic. *Int. J. Soc. Psychiatr.* **2020**, *67*, 54−63.

(2) Kaiser, U. B. Cushing's Disease: Towards Precision Medicine. *Cell Res.* **2015**, *25*, 649−650.

(3) Choudhury, S.; Meeran, K. Glucocorticoid Replacement in Addison Disease. *Nat. Rev. Endocrinol.* **2018**, *14*, 562.

(4) Raul, J.-S.; Cirimele, V.; Ludes, B.; Kintz, P. Detection of Physiological Concentrations of Cortisol and Cortisone in Human Hair. *Clin. Biochem.* **2004**, *37*, 1105−1111.

(5) Anfossi, L.; Tozzi, C.; Giovannoli, C.; Baggiani, C.; Giraudi, G. Development of a Non-Competitive Immunoassay for Cortisol and Its Application to the Analysis of Saliva. *Anal. Chim. Acta* **2002**, *468*, 315−321.

(6) Moore, T. J.; Sharma, B. Direct Surface Enhanced Raman Spectroscopic Detection of Cortisol at Physiological Concentrations. *Anal. Chem.* **2020**, *92*, 2052−2057.

(7) Khan, M. S.; Misra, S. K.; Wang, Z.; Daza, E.; Schwartz-Duval, A. S.; Kus, J. M.; Pan, D.; Pan, D. Paper-Based Analytical Biosensor Chip Designed from Graphene-Nanoplatelet-Amphiphilic-Diblock-Co-Polymer Composite for Cortisol Detection in Human Saliva. *Anal. Chem.* **2017**, *89*, 2107−2115.

(8) Ueno, Y.; Furukawa, K.; Hayashi, K.; Takamura, M.; Hibino, H.; Tamechika, E. Graphene-Modified Interdigitated Array Electrode: Fabrication, Characterization, and Electrochemical Immunoassay Application. *Anal. Sci.* **2013**, *29*, 55−60.

(9) Wu, H.; Ohnuki, H.; Murata, M.; Endo, H. Flow Immunosensor System with an Electrode Replacement Unit for Continuous Cortisol Monitoring for Fish. *Sens. Bio-Sens. Res.* **2017**, *13*, 122−127.

(10) Kim, D.-H.; Viventi, J.; Amsden, J. J.; Xiao, J.; Vigeland, L.; Kim, Y. S.; Blanco, J. A.; Panilaitis, B.; Frechette, E. S.; Contreras, D.; Kaplan, D. L.; Omenetto, F. G.; Huang, Y.; Hwang, K. C.; Zakin, M. R.; Litt, B.; Rogers, J. A. Dissolvable Films of Silk Fibroin for Ultrathin Conformal Bio-Integrated Electronics. *Nat. Mater.* **2010**, *9*, 511−517.
(11) Vepari, C.; Kaplan, D. L. Silk as a Biomaterial. *Prog. Polym. Sci.* **2007**, *32*, 991−1007.
(12) Zhu, B.; Wang, H.; Leow, W. R.; Cai, Y.; Loh, X. J.; Han, M.-Y.; Chen, X. Silk Fibroin for Flexible Electronic Devices. *Adv. Mater.* **2016**, *28*, 4250−4265.
(13) Sun, Q.; Qian, B.; Uto, K.; Chen, J.; Liu, X.; Minari, T. Functional Biomaterials towards Flexible Electronics and Sensors. *Biosens. Bioelectron.* **2018**, *119*, 237−251.
(14) Zhao, G.; Qing, H.; Huang, G.; Genin, G. M.; Lu, T. J.; Luo, Z.; Xu, F.; Zhang, X. Reduced Graphene Oxide Functionalized Nanofibrous Silk Fibroin Matrices for Engineering Excitable Tissues. *NPG Asia Mater.* **2018**, *10*, 982−994.
(15) Zhou, Z.; Shi, Z.; Cai, X.; Zhang, S.; Corder, S. G.; Li, X.; Zhang, Y.; Zhang, G.; Chen, L.; Liu, M.; Kaplan, D. L.; Omenetto, F. G.; Mao, Y.; Tao, Z.; Tao, T. H. The Use of Functionalized Silk Fibroin Films as a Platform for Optical Diffraction-Based Sensing Applications. *Adv. Mater.* **2017**, *29*, 1605471.
(16) Li, Q.; Qi, N.; Peng, Y.; Zhang, Y.; Shi, L.; Zhang, X.; Lai, Y.; Wei, K.; Kim, I. S.; Zhang, K.-Q. Sub-Micron Silk Fibroin Film with High Humidity Sensibility through Color Changing. *RSC Adv.* **2017**, *7*, 17889−17897.
(17) Wang, D.; Wang, L.; Lou, Z.; Zheng, Y.; Wang, K.; Zhao, L.; Han, W.; Jiang, K.; Shen, G. Biomimetic, Biocompatible and Robust Silk Fibroin-MXene Film with Stable 3D Cross-Link Structure for Flexible Pressure Sensors. *Nano Energy* **2020**, *78*, 105252.
(18) Mannoor, M. S.; Tao, H.; Clayton, J. D.; Sengupta, A.; Kaplan, D. L.; Naik, R. R.; Verma, N.; Omenetto, F. G.; McAlpine, M. C. Graphene-Based Wireless Bacteria Detection on Tooth Enamel. *Nat. Commun.* **2012**, *3*, 763.
(19) Munje, R. D.; Muthukumar, S.; Prasad, S. Lancet-Free and Label-Free Diagnostics of Glucose in Sweat Using Zinc Oxide Based Flexible Bioelectronics. *Sens. Actuators, B* **2017**, *238*, 482−490.
(20) Rim, Y. S.; Bae, S.-H.; Chen, H.; Yang, J. L.; Kim, J.; Andrews, A. M.; Weiss, P. S.; Yang, Y.; Tseng, H.-R. Printable Ultrathin Metal Oxide Semiconductor-Based Conformal Biosensors. *ACS Nano* **2015**, *9*, 12174−12181.
(21) Upasham, S.; Thai, K.; Muthyala, R.; Prasad, S. Flexible, Low Volume Detection of Chronobiology Biomarkers from Human Sweat. *Analyst* **2020**, *145*, 784−796.
(22) Lee, M.; Jeon, H.; Kim, S. A Highly Tunable and Fully Biocompatible Silk Nanoplasmonic Optical Sensor. *Nano Lett.* **2015**, *15*, 3358−3363.
(23) Van Baelen, H.; Beck, M.; De Moor, P. A Cortisol-Induced Charge Difference in Desialylated Human Transcortin Detected by Isoelectric Focusing. *J. Biol. Chem.* **1972**, *247*, 2699−2703.
(24) Sekar, M.; Sriramprabha, R.; Sekhar, P. K.; Bhansali, S.; Ponpandian, N.; Pandiaraj, M.; Viswanathan, C. Review—Towards Wearable Sensor Platforms for the Electrochemical Detection of Cortisol. *J. Electrochem. Soc.* **2020**, *167*, 067508.
(25) Kinnamon, D.; Ghanta, R.; Lin, K. C.; Muthukumar, S.; Prasad, S. Portable Biosensor for Monitoring Cortisol in Low-Volume Perspired Human Sweat. *Sci. Rep.* **2017**, *7*, 13312.
(26) Kim, K. H.; Lee, S. H.; Seo, S. E.; Bae, J.; Park, S. J.; Kwon, O. S. Ultrasensitive Stress Biomarker Detection Using Polypyrrole Nanotube Coupled to a Field-Effect Transistor. *Micromachines* **2020**, *11*, 439.
(27) Tlili, C.; Myung, N. V.; Shetty, V.; Mulchandani, A. Label-Free, Chemiresistor Immunosensor for Stress Biomarker Cortisol in Saliva. *Biosens. Bioelectron.* **2011**, *26*, 4382−4386.
(28) Vabbina, P. K.; Kaushik, A.; Pokhrel, N.; Bhansali, S.; Pala, N. Electrochemical Cortisol Immunosensors Based on Sonochemically Synthesized Zinc Oxide 1D Nanorods and 2D Nanoflakes. *Biosens. Bioelectron.* **2015**, *63*, 124−130.
(29) Madhu, S.; Anthuuvan, A. J.; Ramasamy, S.; Manickam, P.; Bhansali, S.; Nagamony, P.; Chinnuswamy, V. ZnO Nanorod Integrated Flexible Carbon Fibers for Sweat Cortisol Detection. *ACS Appl. Electron. Mater.* **2020**, *2*, 499−509.
(30) Tseng, P.; Napier, B.; Garbarini, L.; Kaplan, D. L.; Omenetto, F. G. Functional, RF-Trilayer Sensors for Tooth-Mounted, Wireless Monitoring of the Oral Cavity and Food Consumption. *Adv. Mater.* **2018**, *30*, 1703257.
(31) Wang, X.; Gu, Y.; Xiong, Z.; Cui, Z.; Zhang, T. Silk-Molded Flexible, Ultrasensitive, and Highly Stable Electronic Skin for Monitoring Human Physiological Signals. *Adv. Mater.* **2014**, *26*, 1336−1342.
(32) Wang, C.; Xia, K.; Zhang, M.; Jian, M.; Zhang, Y. An All-Silk-Derived Dual-Mode E-Skin for Simultaneous Temperature-Pressure Detection. *ACS Appl. Mater. Interfaces* **2017**, *9*, 39484−39492.
(33) Park, S. J.; Lee, S. H.; Yang, H.; Park, C. S.; Lee, C.-S.; Kwon, O. S.; Park, T. H.; Jang, J. Human Dopamine Receptor-Conjugated Multidimensional Conducting Polymer Nanofiber Membrane for Dopamine Detection. *ACS Appl. Mater. Interfaces* **2016**, *8*, 28897−28903.
(34) Kim, H.-J.; Park, S. J.; Kim, D.-I.; Lee, S.; Kwon, O. S.; Kim, I. K. Moisture Effect on Particulate Matter Filtration Performance Using Electro-Spun Nanofibers Including Density Functional Theory Analysis. *Sci. Rep.* **2019**, *9*, 7015.
(35) Kwon, O. S.; Park, S. J.; Lee, J. S.; Park, E.; Kim, T.; Park, H.-W.; You, S. A.; Yoon, H.; Jang, J. Multidimensional Conducting Polymer Nanotubes for Ultrasensitive Chemical Nerve Agent Sensing. *Nano Lett.* **2012**, *12*, 2797−2802.
(36) Kim, H.-J.; Park, S. J.; Park, C. S.; Le, T.-H.; Ha, T. H.; Kim, J.; Lee, C.-S.; Yoon, H.; Kwon, O. S. Surface-Modified Polymer Nanofiber Membrane for High-Efficiency Microdust Capturing. *Chem. Eng. J.* **2018**, *339*, 204−213.
(37) Joo, S.; Kim, B.; An, J.; Park, M.; Seo, S.; Park, J. Y.; Bae, J. A Study on Generation of Embossed Carbon Nanopattern by Induced Microdomain Alignments in PAN-Based Block Copolymer under Electric Field. *J. Mater. Sci.* **2018**, *53*, 9316−9324.
(38) Rockwood, D. N.; Preda, R. C.; Yücel, T.; Wang, X.; Lovett, M. L.; Kaplan, D. L. Materials Fabrication from Bombyx Mori Silk Fibroin. *Nat. Protoc.* **2011**, *6*, 1612−1631.
(39) Mannoor, M. S.; Zhang, S.; Link, A. J.; McAlpine, M. C. Electrical Detection of Pathogenic Bacteria via Immobilized Antimicrobial Peptides. *Proc. Natl. Acad. Sci.* **2010**, *107*, 19207−19212.
(40) Kim, D.-H.; Kim, Y.-S.; Amsden, J.; Panilaitis, B.; Kaplan, D. L.; Omenetto, F. G.; Zakin, M. R.; Rogers, J. A. Silicon Electronics on Silk as a Path to Bioresorbable, Implantable Devices. *Appl. Phys. Lett.* **2009**, *95*, 133701.
(41) Kintz, P.; Samyn, N. Chapter 13 Unconventional Samples and Alternative Matrices. *Handb. Anal. Sep.* **2000**, *2*, 459−488.
(42) Mena-Bravo, A.; Luque de Castro, M. D. Sweat: A Sample with Limited Present Applications and Promising Future in Metabolomics. *J. Pharm. Biomed. Anal.* **2014**, *90*, 139−147.
(43) Zhang, Y.; Guo, H.; Kim, S. B.; Wu, Y.; Ostojich, D.; Park, S. H.; Wang, X.; Weng, Z.; Li, R.; Bandodkar, A. J.; Sekine, Y.; Choi, J.; Xu, S.; Quaggin, S.; Ghaffari, R.; Rogers, J. A. Passive Sweat Collection and Colorimetric Analysis of Biomarkers Relevant to Kidney Disorders Using a Soft Microfluidic System. *Lab Chip* **2019**, *19*, 1545−1555.
(44) Yussuf, A.; Al-Saleh, M.; Al-Enezi, S.; Abraham, G. Synthesis and Characterization of Conductive Polypyrrole: The Influence of the Oxidants and Monomer on the Electrical, Thermal, and Morphological Properties. *Int. J. Polym. Sci.* **2018**, *2018*, 1−8.
(45) Pang, S.; Labuza, T. P.; He, L. Development of a Single Aptamer-Based Surface Enhanced Raman Scattering Method for Rapid Detection of Multiple Pesticides. *Analyst* **2014**, *139*, 1895−1901.
(46) Kurouski, D.; Van Duyne, R. P.; Lednev, I. K. Exploring the Structure and Formation Mechanism of Amyloid Fibrils by Raman Spectroscopy: A Review. *Analyst* **2015**, *140*, 4967−4980.

https://doi.org/10.1021/acssensors.1c01734
ACS Sens. 2022, 7, 99−108

(47) Kwon, O. S.; Park, C. S.; Park, S. J.; Noh, S.; Kim, S.; Kong, H. J.; Bae, J.; Lee, C.-S.; Yoon, H. Carboxylic Acid-Functionalized Conducting-Polymer Nanotubes as Highly Sensitive Nerve-Agent Chemiresistors. *Sci. Rep.* **2016**, *6*, 33724.
(48) Sheibani, S.; Capua, L.; Kamaei, S.; Akbari, S. S. A.; Zhang, J.; Guerin, H.; Ionescu, A. M. Extended Gate Field-Effect-Transistor for Sensing Cortisol Stress Hormone. *Commun. Mater.* **2021**, *2*, 10.
(49) Nakatsuka, N.; Yang, K.-A.; Abendroth, J. M.; Cheung, K. M.; Xu, X.; Yang, H.; Zhao, C.; Zhu, B.; Rim, Y. S.; Yang, Y.; Weiss, P. S.; Stojanović, M. N.; Andrews, A. M. Aptamer-Field-Effect Transistors Overcome Debye Length Limitations for Small-Molecule Sensing. *Science* **2018**, *362*, 319−324.
(50) Wang, Y.; Yokota, T.; Someya, T. Electrospun Nanofiber-Based Soft Electronics. *NPG Asia Mater.* **2021**, *13*, 22.
(51) Yang, H.; Kim, D.; Kim, J.; Moon, D.; Song, H. S.; Lee, M.; Hong, S.; Park, T. H. Nanodisc-Based Bioelectronic Nose Using Olfactory Receptor Produced in Escherichia Coli for the Assessment of the Death-Associated Odor Cadaverine. *ACS Nano* **2017**, *11*, 11847−11855.
(52) Liu, Y.; Wang, F.; Liu, Y.; Wang, X.; Xu, Y.; Zhang, R. Charge Transfer at Carbon Nanotube−Graphene van der Waals Heterojunctions. *Nanoscale* **2016**, *8*, 12883−12886.
(53) Jaramillo-Quiceno, N.; Restrepo-Osorio, A. Water-Annealing Treatment for Edible Silk Fibroin Coatings from Fibrous Waste. *J. Appl. Polym. Sci.* **2020**, *137*, 48505.
(54) Park, E.; Kwon, O. S.; Park, S. J.; Lee, J. S.; You, S.; Jang, J. One-Pot Synthesis of Silver Nanoparticles Decorated Poly(3,4-Ethylenedioxythiophene) Nanotubes for Chemical Sensor Application. *J. Mater. Chem.* **2012**, *22*, 1521−1526.
(55) Hwang, Y.; Park, J. Y.; Lee, C.-S.; Kwon, O. S.; Park, S.-H.; Bae, J. Surface Engineered Poly(Dimethylsiloxane)/Carbon Nanotube Nanocomposite Pad as a Flexible Platform for Chemical Sensors. *Composites, Part A* **2018**, *107*, 55−60.
(56) Bae, J.; Hwang, Y.; Park, S.; Ha, J.-H.; Kim, H.; Jang, A.; An, J.; Lee, C.-S.; Park, S.-H. Study on the Sensing Signal Profiles for Determination of Process Window of Flexible Sensors Based on Surface Treated PDMS/CNT Composite Patches. *Polymers* **2018**, *10*, 951.
(57) Jang, H.-J.; Lee, T.; Song, J.; Russell, L.; Li, H.; Dailey, J.; Searson, P. C.; Katz, H. E. Electronic Cortisol Detection Using an Antibody-Embedded Polymer Coupled to a Field-Effect Transistor. *ACS Appl. Mater. Interfaces* **2018**, *10*, 16233−16237.
(58) Dalirirad, S.; Steckl, A. J. Aptamer-Based Lateral Flow Assay for Point of Care Cortisol Detection in Sweat. *Sens. Actuators, B* **2019**, *283*, 79−86.
(59) Kaushik, A.; Yndart, A.; Jayant, R. D.; Sagar, V.; Atluri, V.; Bhansali, S.; Nair, M. Electrochemical Sensing Method for Point-of-Care Cortisol Detection in Human Immunodeficiency Virus-Infected Patients. *Int. J. Nanomed.* **2015**, *10*, 677−685.
(60) Liu, H.; Zhao, H.; Li, S.; Hu, J.; Zheng, X.; Li, R.; Chen, Y.; Su, Y. Adhesion-Free Thin-Film-Like Curvature Sensors Integrated on Flexible and Wearable Electronics for Monitoring Bending of Joints and Various Body Gestures. *Adv. Mater. Technol.* **2019**, *4*, 1800327.
(61) Li, Q.; Li, J.; Tran, D.; Luo, C.; Gao, Y.; Yu, C.; Xuan, F. Engineering of Carbon Nanotube/Polydimethylsiloxane Nanocomposites with Enhanced Sensitivity for Wearable Motion Sensors. *J. Mater. Chem. C* **2017**, *5*, 11092−11099.
(62) Grass, J.; Kirschbaum, C.; Miller, R.; Gao, W.; Steudte-Schmiedgen, S.; Stalder, T. Sweat-Inducing Physiological Challenges Do Not Result in Acute Changes in Hair Cortisol Concentrations. *Psychoneuroendocrinology* **2015**, *53*, 108−116.
(63) Russell, E.; Koren, G.; Rieder, M.; Van Uum, S. H. M. The Detection of Cortisol in Human Sweat: Implications for Measurement of Cortisol in Hair. *Ther. Drug Monit.* **2014**, *36*, 30−34.
(64) Sekar, M.; Pandiaraj, M.; Bhansali, S.; Ponpandian, N.; Viswanathan, C. Carbon Fiber Based Electrochemical Sensor for Sweat Cortisol Measurement. *Sci. Rep.* **2019**, *9*, 403.
(65) Sonmez, B. G.; Ertop, O.; Mutlu, S. Modelling and Realization of a Water-Gated Field Effect Transistor (WG-FET) Using 16-Nm-Thick Mono-Si Film. *Sci. Rep.* **2017**, *7*, 12190.
(66) Ajay; Narang, R.; Saxena, M.; Gupta, M. Modeling and Simulation Investigation of Sensitivity of Symmetric Split Gate Junctionless FET for Biosensing Application. *IEEE Sens. J.* **2017**, *17*, 4853−4861.
(67) Bao, W.; Fang, Z.; Wan, J.; Dai, J.; Zhu, H.; Han, X.; Yang, X.; Preston, C.; Hu, L. Aqueous Gating of van Der Waals Materials on Bilayer Nanopaper. *ACS Nano* **2014**, *8*, 10606−10612.
(68) Koh, L.-D.; Cheng, Y.; Teng, C.-P.; Khin, Y.-W.; Loh, X.-J.; Tee, S.-Y.; Low, M.; Ye, E.; Yu, H.-D.; Zhang, Y.-W.; Han, M.-Y. Structures, Mechanical Properties and Applications of Silk Fibroin Materials. *Prog. Polym. Sci.* **2015**, *46*, 86−110.
(69) Perrone, G. S.; Leisk, G. G.; Lo, T. J.; Moreau, J. E.; Haas, D. S.; Papenburg, B. J.; Golden, E. B.; Partlow, B. P.; Fox, S. E.; Ibrahim, A. M.; Lin, S. J.; Kaplan, D. L. The Use of Silk-Based Devices for Fracture Fixation. *Nat. Commun.* **2014**, *5*, 3385.
(70) Wang, Q.; Jian, M.; Wang, C.; Zhang, Y. Carbonized Silk Nanofiber Membrane for Transparent and Sensitive Electronic Skin. *Adv. Funct. Mater.* **2017**, *27*, 1605657.

https://doi.org/10.1021/acssensors.1c01734
ACS Sens. 2022, 7, 99−108